Journal of The Electrochemical Society, 155 (10) G203-G208 (2008)
0013-4651/2008/155(10)/G203/6/$23.00 © The Electrochemical Society

Characteristics of Atomic-Layer-Deposited Al_2O_3 High-*k* Dielectric Films Grown on Ge Substrates

Chao-Ching Cheng,[a] Chao-Hsin Chien,[a,b,z] Guang-Li Luo,[b] Jun-Cheng Liu,[a] Chi-Chung Kei,[c] Da-Ren Liu,[c] Chien-Nan Hsiao,[c] Chun-Hui Yang,[b] and Chun-Yen Chang[a]

[a]*Institute of Electronics, National Chiao-Tung University, Hsinchu, 300 Taiwan*
[b]*National Nano Device Laboratory, Hsinchu, 300 Taiwan*
[c]*Instrument Technology Research Center, National Applied Research Laboratories, Hsinchu, 300 Taiwan*

This paper describes the structural and electrical properties of Al_2O_3 thin films grown through atomic layer deposition onto Ge substrates over a wide deposition temperature range (50–300°C). From grazing-incidence X-ray reflectivity and X-ray photoelectron spectroscopy, we found that increasing the deposition temperature improved the Al_2O_3 film density and its dielectric stoichiometry; nevertheless, dielectric intermixing between main Al_2O_3 and interfacial GeO_2 appeared at temperatures above 200°C, along with degradation of the GeO_2/Ge interface. Accordingly, a relatively large gate leakage current (J_g) and a high density of interfacial states D_{it} ($>10^{13}$ cm^{-2} eV^{-1}) were observed as a result of deterioration of the entire Al_2O_3/Ge structure at higher deposition temperatures. In addition, although subsequent high-temperature processing at 600°C in a N_2 ambient could relieve the oxygen-excessive behavior further, i.e., to provide a more stoichiometric film, the accompanying GeO_x volatilization close to the dielectric interface caused greater damage to the electrical performance. Only forming gas annealing (H_2/N_2, 1:10) at low temperature (300°C) improved the capacitance–voltage characteristics of the Pt/Al_2O_3/Ge structure, in terms of providing a lower value of D_{it} (ca. 6×10^{11} cm^{-2} eV^{-1}), a lower value of J_g, and a reduced hysteresis width.
© 2008 The Electrochemical Society. [DOI: 10.1149/1.2965495] All rights reserved.

Manuscript submitted March 21, 2008; revised manuscript received June 16, 2008. Published August 19, 2008.

High-*k* Al_2O_3 is considered a potential alternative gate dielectric material on Si substrates for application to metal oxide semiconductor field-effect transistors (MOSFETs) because of its wide bandgap energy (ca. 8.8 eV), large conduction/valance band offsets, and high thermodynamic stability. Nevertheless, there are several drawbacks affecting the deposition of Al_2O_3 on Si, relative to SiO_2, including the low crystallization temperature, the high thermal expansion coefficient, and the high densities of negative fixed charges and interface states (D_{it}). Recent progress in the deposition of high-*k* materials, e.g., the use of deposition techniques such as atomic layer deposition (ALD), has meant that some of these problems can be overcome.[1] Several reports have described the characteristics of ALD-Al_2O_3 dielectric films grown on Si using trimethylaluminum [TMA, $Al(CH_3)_3$] as the precursor and H_2O as the oxidant because of the excellent ALD mechanism and broad process window.[2,3] In recent years, many investigators have studied the deposition of ALD-HfO_2 high-*k* layers on high-mobility Ge substrates[4] using a variety of oxidants[5] in efforts aimed at enhancing the driving current in MOSFETs. Meanwhile, various surface preparation techniques, e.g., the incorporation of ultrathin Si,[6,7] AlN_x, and GeON dielectric interlayers,[8,9] plasma treatment with NH_3 or PH_3,[10,11] and chemical passivation[12] with $(NH_4)_2S$, have been developed to enhance the electrical performance of Ge capacitors and transistors[13] because the primary obstacle affecting the fabrication of high-*k*/Ge structures is the presence of GeO_x native oxides and their thermal desorption, which debases the Ge device characteristics, e.g., to provide a high value of D_{it}, a large gate leakage current, and severe charge trapping. In this study, we analyzed the composition and interfacial chemistry of an ALD-Al_2O_3 dielectric deposited on a bulk Ge substrate at temperatures in the range of 50–300°C; subsequent thermal processing strongly influenced the structural stability and electrical properties of the Al_2O_3/Ge system.

Experimental

The p-Ge substrate had a doping concentration of ca. 2×10^{15} cm^{-3} (resistivity ca. 2 Ω cm). The split samples were etched in HF solutions of various concentrations; the surface roughness was measured using atomic force microscopy (AFM) over a scanning area of 1×1 μm. The optimal wet-chemical cleaning (Fig. 1) method, involving cyclical rinsing with deionized (DI) water and dilute HF solution (HF/DI water, 1:30) for 5 and 1 min, respectively, was performed prior to dielectric film deposition. The Al_2O_3 thin films were subsequently grown on the bulk Ge at substrate temperatures of 50, 100, 200, and 300°C, respectively, while maintaining the chamber pressure at 10 Torr in the ALD system. $Al(CH_3)_3$ and H_2O were chosen as the Al metal source and oxidant, respectively; they were pulsed alternately into the reactor for 1 s per pulse, separated by a N_2 purge of 10 s to remove redundant reactants. Next, a 700 Å thick layer of Pt was deposited using a sputtering system to pattern the capacitor electrode through the shadow mask. Two post-thermal processes were tested: (*i*) rapid thermal annealing (RTA) at 400 or 600°C in a N_2 ambient for 30 s and (*ii*) forming gas annealing (FGA) at 300°C in a H_2/N_2 (10%) mixed ambient for 30 min. Finally, a thermal coater was used to deposit Al as the back-side contact. Optical microscopy revealed that the gate capacitance area was ca. 4×10^{-4} cm^2.

Physical analyses: high-resolution transmission electron microscopy (TEM), secondary-ion mass spectroscopy (SIMS), grazing-

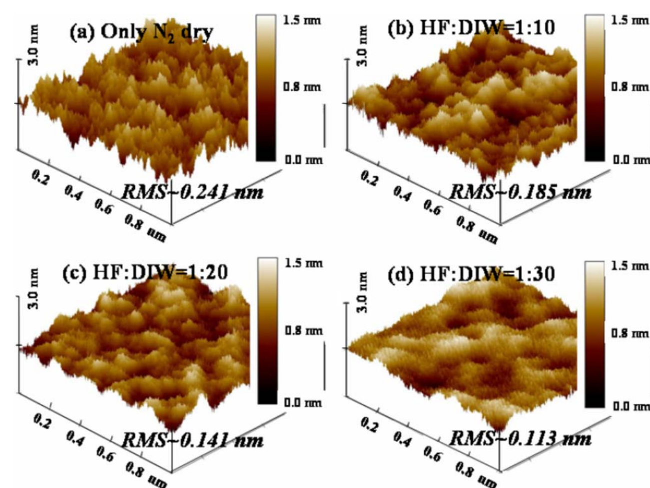

Figure 1. (Color online) AFM images of the etched Ge substrate subjected to HF solutions of three different concentrations.

[z] E-mail: chchien@faculty.nctu.edu.tw

Downloaded on 2014-04-25 to IP 140.113.38.11 address. Redistribution subject to ECS terms of use (see ecsdl.org/site/terms_use) unless CC License in place (see abstract).

incidence X-ray reflectivity (GI-XRR), and X-ray photoelectron spectroscopy (XPS), were performed to investigate the as-deposited Al_2O_3/Ge structure and its compositional variation after thermal annealing. The GI-XRR system employed parallel collimated and monochromatic beams (Cu Kα radiation; λ = 1.5406 Å) and a scanned angle ranging from 0 to 7600 arc. The reflected X-ray signal was analyzed using a commercial Bede REFS Mercury software package based on the four-layered stack model; the available data in experiments were applied to minimize the cost function χ^2 and more accurately extract all the parameters during curve fitting. For XPS analysis, an Al Kα excitation source operating at 1486.6 eV was employed to collect the photoelectrons at a take-off angle of 60° with respect to the surface horizontal. These measurements allowed us to examine not only the density and stoichiometry of the Al_2O_3 dielectric films but also the interfacial GeO_x chemistry and thermal diffusion behavior within the high-*k* dielectric. For electrical characterization, the parallel capacitance–voltage (*C-V*), parallel conductance–voltage, and gate leakage impurity vacancy (*I-V*) behavior of Pt/ALD-Al_2O_3/p-Ge metal-oxide semiconductor (MOS) structures were measured. Nicollian and Goetzberger's conductance method considering the fluctuation of surface band bending was used to determine the value of D_{it}.[14]

Results and Discussion

Physical properties of ALD-Al_2O_3/Ge structures.— Figures 1a-d display AFM images of the Ge surface before and after cyclical HF wet-chemical cleaning; the surface morphology improved upon decreasing the HF concentration. The root-mean-square roughness decreased from 0.241 to 0.113 nm after dilute HF etching (HF/DI water, 1:30), i.e., to a value comparable to the common value of ca. 0.1 nm obtained for a HF-last Si wafer. In contrast to Si, however, the hydrophobic behavior of Ge gradually diminishes as either the acid concentration decreases or the exposure time in air increases, and it disappears after rinsing in DI water again. Two possible mechanisms might be responsible for this behavior: (*i*) Ge–H bonds are weaker than Ge–OH bonds, as evidenced by their respective binding energies of 4.6–4.9 and 5.6–5.8 eV;[15] the reversibility of the chemical transformation of GeH into GeOH has also been characterized.[16] (*ii*) The contamination of GeC-based carbide species, rather than a pure GeH surface coverage, can occur within a few minutes in air, thereby resulting in a hydrophilic Ge surface.[17]

The TEM images in Fig. 2a-d reveal that the thicknesses of as-deposited Al_2O_3 thin films on Ge substrate were dependent on the deposition temperature (T_{dep}); they were ca. 53, 62, 70, and 48 Å after 60 deposition cycles at values of T_{dep} of 50, 100, 200, and 300°C, respectively. The Al_2O_3 exhibited an amorphous phase in these samples, but we did not observe the existence of an obvious interfacial layer; nevertheless, the oxygen atoms are likely to react with the Ge substrate surface during deposition, probably in the form of GeO_x species, because Ge is readily oxidized. A blurred oxide–substrate interface became apparent upon increasing the value of T_{dep} to above 200°C, presumably correlating with the interfacial GeO_x desorption; the detailed surface chemistry is discussed in the following sections describing the XRR and XPS analyses. Figure 3 displays a plot of the corresponding ALD-Al_2O_3 deposition rate on Ge determined in this study, together with those on Si as reported by Ott et al.[2] and Groner et al.;[3] the results indicate a similar ALD growth behavior with respect to the value of T_{dep}. Meanwhile, these experimental data were simulated well using our proposed ALD model,[18] suggesting that the growth mechanism was mainly determined by the activation energy in Al_2O_3 chemical reactions at low temperatures and by the adsorption coverage of AlOH* or $Al(CH_3)$* reactive species at high temperatures. These two effects ensured that the growth rate achieved a maximum at a critical temperature (T_{max}); in our case, the value of T_{max} was ca. 170°C, close to the value (ca. 175°C) reported by Ott et al., but higher than that (ca. 125°C) observed by Groner et al. The resultant shift of the value of T_{max} was correlated to differences in the chemisorption energy required for Al_2O_3 deposition as well as the desorption rate of formed surface species; further details of this behavior are described elsewhere.[18]

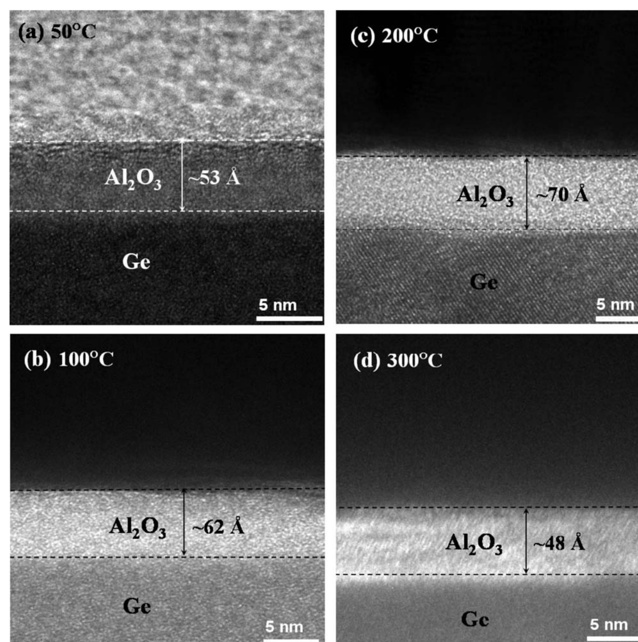

Figure 2. TEM images of the as-deposited Pt/ALD-Al_2O_3/Ge structure after 60 deposition cycles under different values of T_{dep}.

Figure 4a compares the XRR curves of Al_2O_3/Ge samples deposited at 50 and 300°C. The four-layer model of the $Al_2O_3/Ge_xAl_{1-x}O/GeO_2$/Ge gate stack fit the measured curve nearly perfectly; note that the presence of a $Ge_xAl_{1-x}O$ interlayer, arising from the intermixing of Al_2O_3 and GeO_2, had to be considered in the model to accomplish an excellent fit to the curve. The oscillation frequency is determined primarily by the thickness of the overlying Al_2O_3 film, and the oscillation amplitude is very sensitive to the variation in roughness between the top surface and the deposited interface. The 300°C Al_2O_3 on the Ge substrate exhibited a slower oscillation frequency with a higher amplitude variation, reflecting its thinner Al_2O_3 film and rougher Ge interface, with respect to those of the substrate prepared at 50°C. Note that the top surface roughness (<3 Å) was similar in all samples. We also observed that the peak

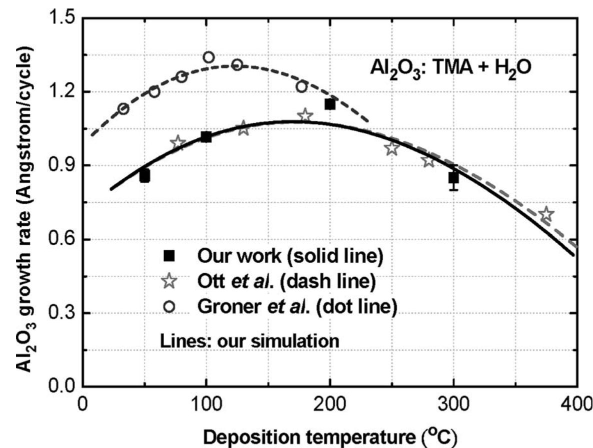

Figure 3. Growth rates of ALD-Al_2O_3 films plotted against the value of T_{dep} for both this and previous studies (by Ott et al. and Groner et al.). Solid lines represent the simulation of our proposed ALD model (Ref. 18).

Downloaded on 2014-04-25 to IP 140.113.38.11 address. Redistribution subject to ECS terms of use (see ecsdl.org/site/terms_use) unless CC License in place (see abstract).

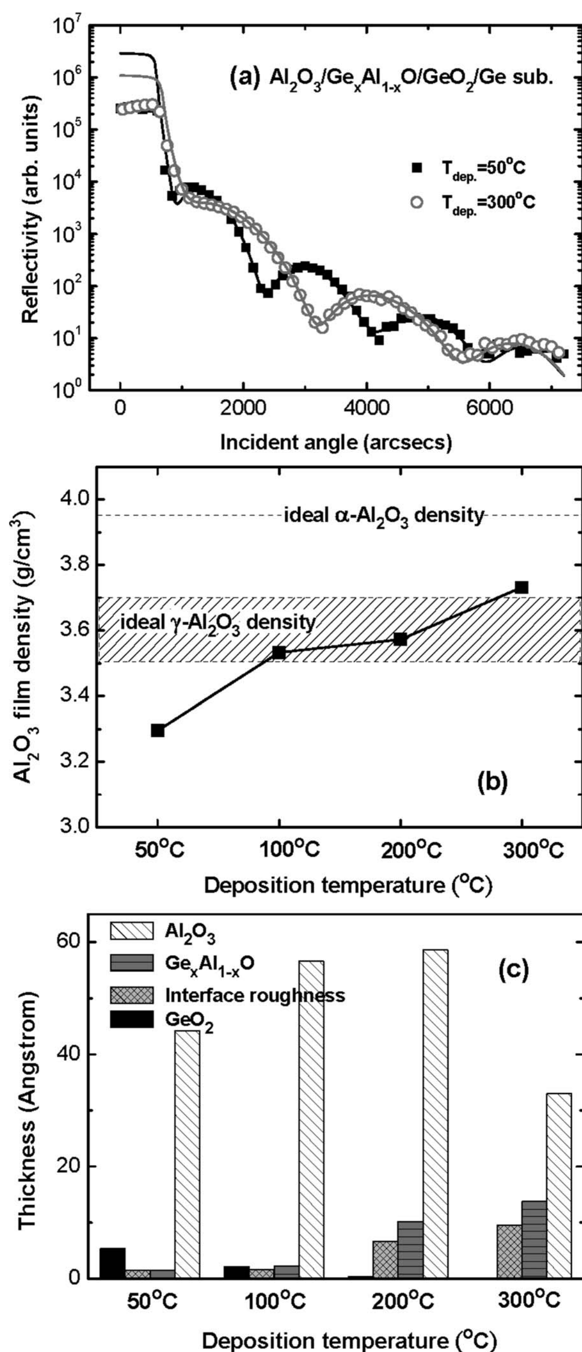

Figure 4. (a) Measured and simulated GI-XRR curves of the as-deposited Al_2O_3 (60 cycles)/Ge structures at values of T_{dep} of 50 and 300°C. (b) Extracted Al_2O_3 film densities plotted with respect to the value of T_{dep}. (c) Extracted thicknesses of each layer and GeO_2/Ge interface roughness plotted against the value of T_{dep}. Note that the modeled XRR structure is the $Al_2O_3/Ge_xAl_{1-x}O/GeO_2$/Ge gate stack.

positions of the maxima shifted with the incident angle in these two samples, a typical effect of the Al_2O_3 density changing with the value T_{dep}. Indeed, the film density increased from ca. 3.3 to ca. 3.7 g cm^{-3} (Fig. 4b). Compared with the high density (3.97 g cm^{-3}) of crystalline α-Al_2O_3,[19] the density of each as-deposited Al_2O_3 film was indeed closer to those reported for γ-Al_2O_3 or amorphous alumina (3.5–3.7 g cm^{-3}).[19,20] The lower densities of the Al_2O_3 films observed upon decreasing the value of T_{dep} arose mainly from the thermally activated reaction kinetics dominating at lower temperatures, especially because we used TMA and H_2O in the ALD

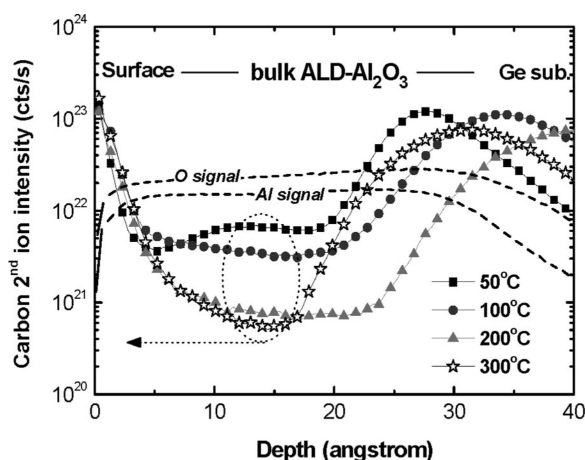

Figure 5. SIMS depth profiles of carbon second-ion intensity within ALD-Al_2O_3 (60 cycles) on Ge substrate deposited at various values of T_{dep}. The Al and O second-ion intensities of the Al_2O_3 (T_{dep} = 300°C)/Ge sample are labeled as a reference of the relative depth.

process, which caused an increase in the levels of H, OH, and C impurities in films. Using forward recoil spectrometry, the hydrogen concentration in ALD-Al_2O_3 has been observed to increase upon decreasing the value of T_{dep} from 175 to 35°C.[3] SIMS analyses (Fig. 5) provided further evidence for a relatively large carbon concentration within the main Al_2O_3 prepared at temperatures below T_{max}, i.e., $<$200°C. When excess O atoms or the C/H contaminants were present within the Al_2O_3, probably in the form of aluminum hydroxide [$Al(OH)_3$] and aluminum oxyhydroxide, the densities of which are 2.42 and 3.44 g cm^{-3}, respectively,[21] the film density was lowered accordingly.

Figure 4c depicts the respective thicknesses of main Al_2O_3, mixed Al_2O_3–GeO_2, and interfacial GeO_2 layers after 60 deposition cycles as a function of T_{dep}; at first, the overall XRR thicknesses were close to the TEM observations. Interestingly, as the value of T_{dep} increased from 50 to 300°C, the thickness of the underlying GeO_2 layer decreased gradually from ca. 5 Å to below 1 Å, whereas that of the intermediate $Ge_xAl_{1-x}O$ layer increased dramatically from ca. 1 to ca. 14 Å, accompanied by an increased roughness between the GeO_2 layer and Ge substrate. These structural degradations became severe at temperatures above 200°C, implying that, during ALD deposition, the poorly oxidized GeO_x species at the surface were less stable and probably diffused into the top Al_2O_3 at higher values of T_{dep}, leading to a more severe dielectric intermixing and degraded interfacial roughness. Seo et al. speculated that a similar behavior occurred during the growth of HfO_2 thin films on Ge substrates using molecular beam epitaxy;[22] they observed that the surface GeO_x species possibly dissolve in HfO_2 at a growth temperature of 360°C.

Next, we examined the relevance of the Al 2p and O 1s photoemission spectra, in particular their peak energy spacing; Fig. 6a provides an example of the as-deposited Al_2O_3/Ge. The value of the energy spacing was ca. 456.95 eV, close to the value of 457 eV for sapphire, but we did not observe a correlation between the energy spacing and the deposition temperature because the chemical shift was within 1 eV. Therefore, we further investigated the stoichiometry of the temperature-dependent grown Al_2O_3 before and after rapid thermal processing (Fig. 6b). Two noteworthy features are that (*i*) the O/Al composition ratio gradually achieved the ideal value of 1.5 upon increasing the value of T_{dep} to 200°C, but it increased to 1.65 at 300°C, and (*ii*) a more stoichiometric film was formed after subsequent RTA. We can explain the variation of the O/Al composition ratio reasonably in terms of the controlled growth mechanism. As we mentioned earlier, raising the value of T_{dep} led to redundant oxygen-based radicals being expelled from the deposited films,

Downloaded on 2014-04-25 to IP 140.113.38.11 address. Redistribution subject to ECS terms of use (see ecsdl.org/site/terms_use) unless CC License in place (see abstract).

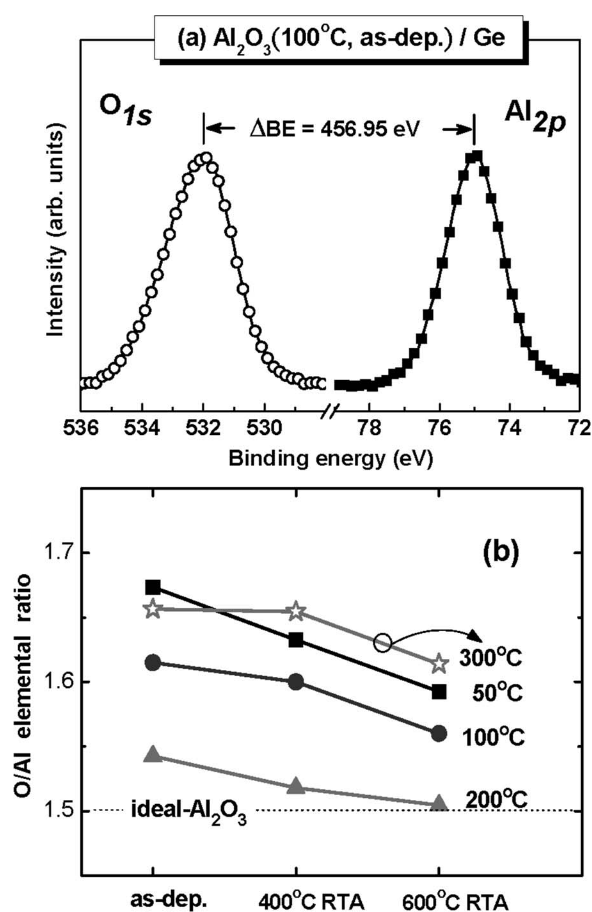

Figure 6. (a) Binding energy difference between the peak positions of Al 2p and O 1 s core levels for the as-deposited Al_2O_3 (T_{dep} = 100°C)/Ge structure. (b) Oxygen-to-aluminum elemental ratios estimated from the respective photoemissions of the Al_2O_3 (T_{dep} = 50–300°C)/Ge samples subjected to RTA at 400 and 600°C, respectively.

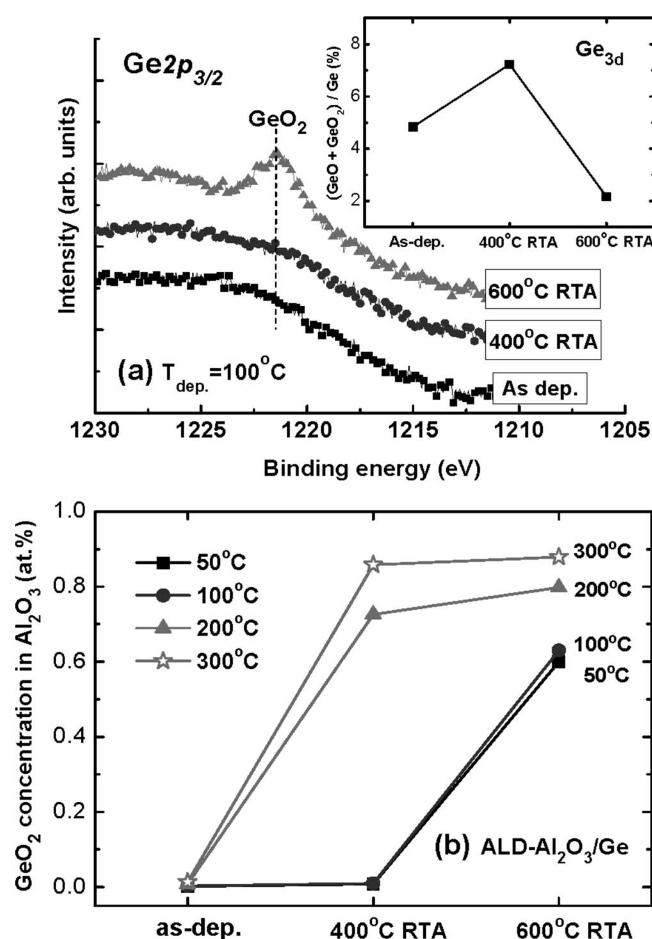

Figure 7. (a) Ge $2p_{3/2}$ core level spectra of the Al_2O_3 (T_{dep} = 100°C)/Ge structure before and after RTA. Inset: Emission ratio of Ge oxides to substrate extracted from the Ge 3d core level. (b) Calculated GeO_2 atomic concentration within Al_2O_3 high-*k* dielectric (T_{dep} = 50–300°C) grown on Ge substrate before and after RTA.

which in turn suppressed the oxygen content and, thus, improved the Al_2O_3 stoichiometry. Above T_{max} (ca. 180°C), the deposition process relies strongly on the presence of AlOH* or $Al(CH_3)$* reactive sites because of the lower adsorption rate. In other words, a relatively higher H_2O concentration exists close to the surface at higher T_{dep}, presumably leading to the oxygen-excessive Al_2O_3 film observed when T_{dep} was 300°C. A similar tendency was also characterized in the electrical permittivity, ca. 5.1, 6.2, 7.9, and 5.8 for as-deposited Al_2O_3 films grown at T_{dep} of 50, 100, 200, and 300°C, respectively; a relatively higher value was obtained at 200°C. Furthermore, we suggest that high-temperature annealing provides additional thermal energy, acting as an external driving force, to return these as-deposited Al_2O_3 samples to their stable, stoichiometric phase.

GeO_x out-diffusion after thermal annealing is a critical issue in the preparation of high-*k*/Ge structures. Surface-sensitive Ge $2p_{3/2}$ spectroscopy (Fig. 7a) revealed that no Ge oxides diffused into the top of the Al_2O_3 dielectric after 400°C RTA, but the bulk-sensitive Ge 3d spectrum (inset) revealed an increased GeO_x/Ge intensity ratio, indicative of GeO_2 growth near the lower interface. When we increased the RTA temperature to 600°C, we detected a small peak corresponding to GeO_2 in the Ge $2p_{3/2}$ spectrum along with a reduced GeO_x/Ge ratio in the Ge 3d spectrum. We speculate that the balance between two competing processes, oxide growth and oxide desorption, which are strongly dependent on both the temperature and oxygen concentration, determines the amount of residual Ge oxide and its distribution. Because we used a N_2 ambient as the feed gas, oxide desorption (rather than oxide growth) should dominate the thermal reaction mechanism. Together with the finding that the critical temperature of GeO desorption was in the range of 360–425°C,[23,24] it is probable that GeO_2 continued to grow at ca. 400°C due to the presence of some residual oxygen in the N_2 ambient, but it most likely desorbed at the higher temperature of 600°C. In Fig. 7b, the Al_2O_3/Ge deposited at a lower temperature of 50°C exhibited results similar to that deposited at 100°C after RTA; moreover, the higher-temperature Al_2O_3 samples appeared to display a lower resistivity in GeO_x incorporation. Note that the calculated value of the GeO_2 atomic concentration in Al_2O_3, based on a standard sampling depth of ca. 30 (±4) Å for the Ge 2 $p_{3/2}$ spectrum, might be affected by different Al_2O_3 overlaying thicknesses in these samples. Here, the GeO_2 concentration remained low (<1.0 atom %) in all cases. In view of the earlier XRR examination, the as-deposited Al_2O_3/Ge structures displayed an increased $Ge_xAl_{1-x}O$ intermixing phenomenon, especially at temperatures up to 200°C. Therefore, we conclude that high-temperature annealing is likely to cause interfacial GeO_x volatilization on the bottom of the Al_2O_3 dielectric with a small degree of Ge incorporation. It was suspected that Al_2O_3/Ge capacitors undergoing RTA at 600°C might suffer from resultant dielectric intermixing, as in the case of the high-T_{dep} systems (≥200°C); indeed, both the interface quality and the leakage current characteristics deteriorated (data not shown). These ex-

Downloaded on 2014-04-25 to IP 140.113.38.11 address. Redistribution subject to ECS terms of use (see ecsdl.org/site/terms_use) unless CC License in place (see abstract).

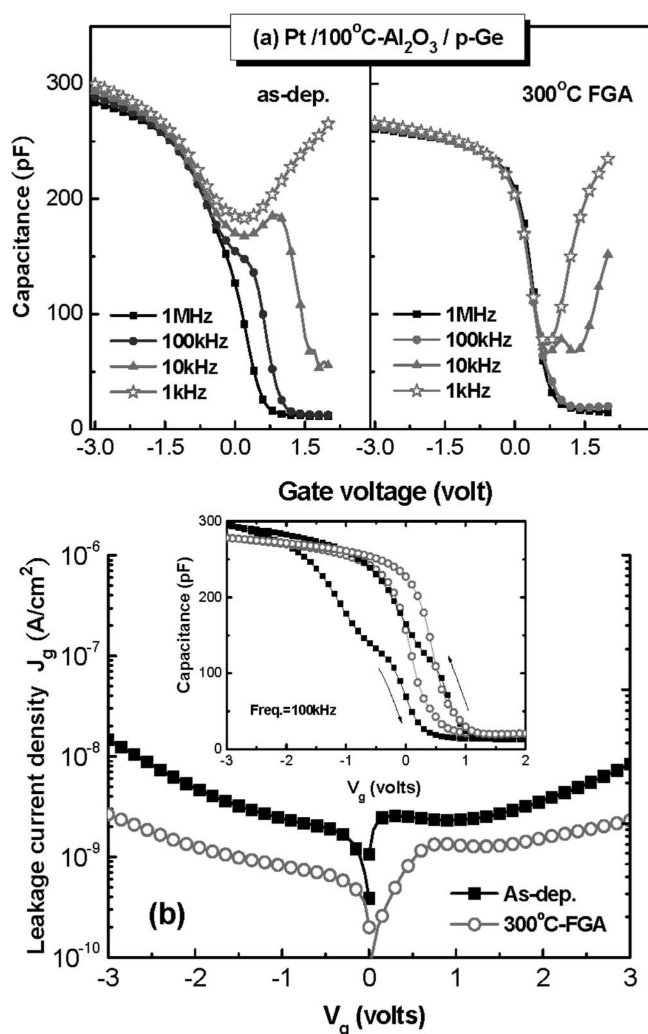

Figure 8. (a) Multifrequency *C-V* and (b) *I-V* characteristics of the Pt/Al_2O_3 (T_{dep} = 100°C)/p-Ge MOS capacitors before and after FGA at 300°C. Inset: Bidirectional *C-V* curves measured at 100 kHz.

perimental findings agree with those of previous studies suggesting that the volatilization of gaseous GeO into high-*k* layers degrades the insulator properties.[6,25]

Electrical characteristics of ALD-Al_2O_3/Ge structure.— The physical analyses described above suggested that Al_2O_3 ALD films grown on p-Ge substrates at the T_{dep} range of 100–200°C should exhibit improved dielectric and interfacial qualities. Thus, we studied the electrical properties of Ge MOS capacitors incorporating Al_2O_3 deposited at 100°C; Fig. 8a depicts the multifrequency *C-V* curves recorded before and after FGA at 300°C. Note that the *C-V* sweep direction presented here was from strong inversion to strong accumulation, and that the as-deposited Al_2O_3 thickness increased to ca. 80 Å in this case. For the as-deposited sample, we observed *C-V* stretch-out behavior along with humps that emerged in the depletion and weak inversion regimes, arising from the onset of surface slow states. Subsequent FGA processing improved the quality of the Al_2O_3-Ge interface, such that the *C-V* curves reached full accumulation saturation with a deeper "dip" in depletion, i.e., the deviation of the 1 kHz curve was diminished with respect to that of the 1 MHz curve. Another noticeable phenomenon is the significant frequency dispersion in the strong inversion region, which is consistent with a high intrinsic carrier concentration and a large density of bulk traps close to the midgap in Ge; consequently, a fast accumulation of minority carriers could occur at the Ge surface.[26] Vanhellemont and Simoen reported that metal impurities, in particular Fe and Ni, are responsible for these deep levels, with a trap energy of ca. 0.3 eV within the bandgap.[27] From electrical characterization, the trap density was estimated to be ca. 10^{15}–10^{16} cm^{-3} in the bulk Ge substrate.[28] Figure 8b provides a comparison of the *I-V* characteristics; the inset presents the bidirectional sweep of the *C-V* curves. At a similar value of the capacitance equivalent thickness, the value of J_g and the degree of charge trapping were both reduced after FGA; we attribute these improvements to the resultant passivation of the interfacial traps.

The common approaches toward extracting the value of D_{it} for Si MOS capacitors, namely the Terman,[29] high-low frequency capacitance,[30] and conductance[12] methods, cannot be fully applied to Ge devices because carrier exchange between the interface states and the minority-carrier bandedge influences the D_{it} extraction in the weak inversion regime.[28] Here, the statistical conductance model was utilized to evaluate the energy distribution of D_{it} only within the limited gate biases. Figure 9a provides a plot of the conductance (G_p/ω) as a function of the measured frequency (f_m) for the as-deposited Al_2O_3/Ge capacitor under gate biases ranging from 0.2 to 0.7 V, i.e., where the device is biased from depletion to weak inversion. During the D_{it} extraction, only the conductance peak having the shoulder near the higher-frequency side was fitted well. Most importantly, two interesting features appeared upon increasing the positive gate bias: (*i*) the G_p/ω peak increased in intensity gradually and moved to lower frequency and (*ii*) the plateau in the range 1–10 kHz had a higher magnitude. As it is well known, two main physical mechanisms are responsible for the onset of the ac conductance loss peak: (*i*) the carrier transition between the interface states near the Fermi level and the majority-carrier bandedge, which certainly dominates at gate bias in depletion, and (*ii*) the dark current of the minority carriers that charge the inversion layer; they arise not only from the bulk traps within the depletion layer but also from the diffusion current from the bulk semiconductor. Based on the observation that the generation and recombination of the bulk traps over the diffusion mechanism contributed to the main minority-carrier current at temperatures below ca. 45°C,[26] we suppose that in the weak inversion region the competition between bulk trap loss and interface state loss is intense. The resultant shift of the gate bias-dependent G_p/ω peak reflected the fact that charging and discharging of the interface traps should dominate these energy losses. As for the conductance plateau observed on the lower-frequency side (1–10 kHz), Evangelou et al. successively simulated this anomalous behavior using the continuum D_{it} model accompanying the tunneling effect of the majority carriers from the semiconductor surface to the bulk oxide defects.[30] We suspect, however, that the insensitive conductance loss should be strongly related to the intrinsic properties of Ge; studies of temperature- and doping concentration dependences are currently under investigation.

In terms of the frequency-dependent conductance peaks, Fig. 9b reveals the change in D_{it} after thermal processing. The value of D_{it} of the as-deposited sample was ca. 4×10^{12} cm^{-2} eV^{-1}; it increased to ca. 2×10^{13} cm^{-2} eV^{-1} after RTA at 600°C, but decreased to ca. 5×10^{11} cm^{-2} eV^{-1} after FGA at 300°C, indicating that the low-temperature FGA did help to repair the high-*k*–Ge interface.[31] The in-diffused hydrogen possibly filled the existed defects inside poor-quality GeO_x between the high-*k*/Ge interface.[32] In addition, as is evident in Fig. 9c, the employed value of T_{dep} was also a determining factor affecting the quality of the interface between the grown Al_2O_3 and Ge. Apparently, the value of D_{it} increased to greater than 10^{13} cm^{-2} eV^{-1} when T_{dep} was 200 and 300°C, showing consistency with the results of appreciable interfacial dielectric intermixing. In other words, it is essential to protect the Ge devices from GeO_x formation and volatilization under either higher-temperature deposition or higher-temperature post-thermal processing to achieve the optimal electrical performance.

Downloaded on 2014-04-25 to IP 140.113.38.11 address. Redistribution subject to ECS terms of use (see ecsdl.org/site/terms_use) unless CC License in place (see abstract).

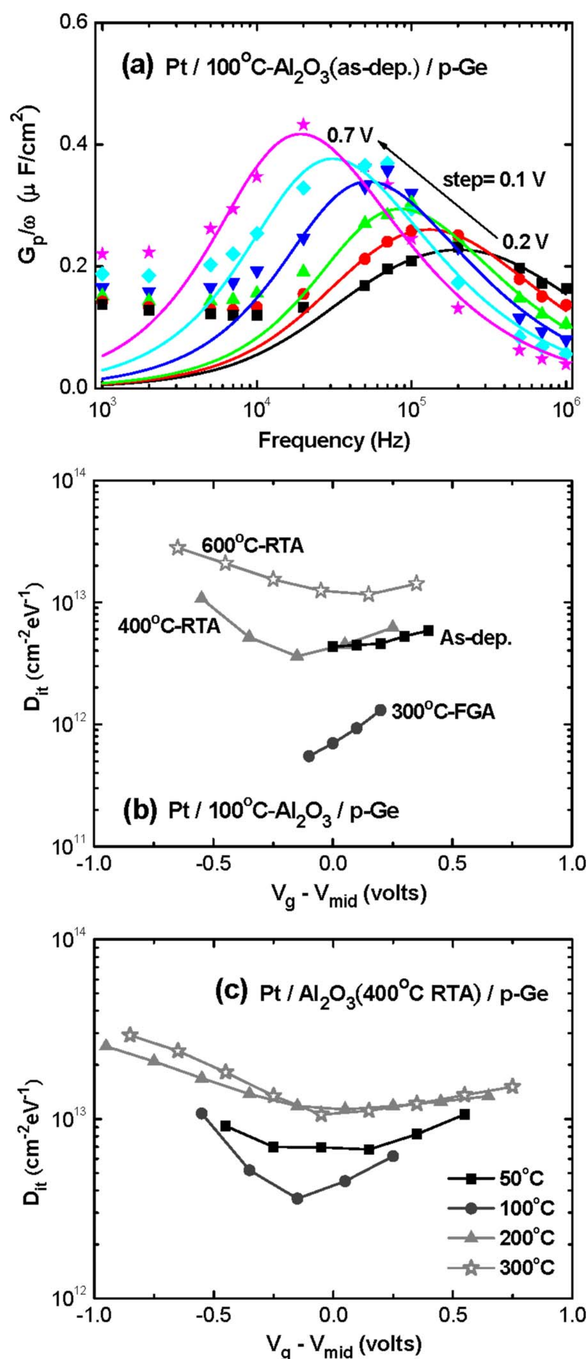

Figure 9. (Color online) (a) Plot of G_p/ω vs the log frequency curves for the as-deposited Pt/Al_2O_3 (T_{dep} = 100°C)/p-Ge structure under various gate biases. Energy distribution of D_{it} for Pt/Al_2O_3/p-Ge samples (b) subjected to different thermal processing and (c) grown at values of T_{dep} from 50 to 300°C.

Conclusions

We have characterized the dielectric and interface qualities of ALD-Al_2O_3 thin films grown on Ge substrates over a values of T_{dep} ranging from 50 to 300°C. GI-XRR and XPS measurements revealed that increasing the value of T_{dep} enhanced the Al_2O_3 film density and its dielectric stoichiometry, but temperatures above 200°C led to the formation of a $Ge_xAl_{1-x}O$ intermediate layer through the intermixing of Al_2O_3 and GeO_2, which damaged the GeO_2–Ge interface. Therefore, a relatively large value of J_g and an increased value of D_{it} ($>10^{13}$ cm^{-2} eV^{-1}) arose from structural deterioration in Al_2O_3/Ge at higher values of T_{dep}. Although N_2 RTA at 600°C abated the resultant oxygen-excessive behavior, i.e., providing a more stoichiometric film, interfacial GeO_x volatilization resulted in the greater electrical degradation. In contrast, FGA at 300°C improved the *C-V* curves of Pt/Al_2O_3/Ge MOS capacitors, including lower values of D_{it} (ca. 6×10^{11} cm^{-2} eV^{-1}) and J_g and reduced hysteresis width.

Acknowledgment

This study was sponsored primarily by the National Science Council of Taiwan (contract no. NSC94-2215-E009-066).

National Chiao-Tung University assisted in meeting the publication costs of this article.

References

1. S. K. Kim, S. W. Lee, C. S. Hwang, Y.-S. Min, J. Y. Won, and J. Jeong, *J. Electrochem. Soc.*, **153**, F69 (2006).
2. A. W. Ott, J. W. Klaus, J. M. Johnson, and S. M. George, *Thin Solid Films*, **292**, 135 (1997).
3. M. D. Groner, F. H. Fabreguette, J. W. Elam, and S. M. George, *Chem. Mater.*, **16**, 639 (2004).
4. C. O. Chui, H. Kim, D. Chi, P. C. McIntyre, and K. C. Saraswat, *IEEE Trans. Electron Devices*, **53**, 2551 (2006).
5. S. Spiga, C. Wiemer, G. Tallarida, G. Scarel, S. Ferrari, G. Seguini, and M. Fanciulli, *Appl. Phys. Lett.*, **87**, 112904 (2005).
6. W. P. Bai, N. Lu, and D.-L. Kwong, *IEEE Electron Device Lett.*, **26**, 378 (2005).
7. N. Wu, Q. Zhang, C. Zhu, D. S. H. Chan, A. Du, N. Balasubramanian, M. F. Li, A. Chin, and J. K. O. Sin, *IEEE Electron Device Lett.*, **25**, 631 (2004).
8. F. Gao, S. J. Lee, J. S. Pan, L. J. Tang, and D.-L. Kwong, *Appl. Phys. Lett.*, **86**, 113501 (2005).
9. W. P. Bai, N. Lu, A. P. Ritenour, M. L. Lee, D. A. Antoniadis, and D.-L. Kwong, *IEEE Trans. Electron Devices*, **53**, 2551 (2006).
10. C.-C. Cheng, C.-H. Chien, G.-L. Luo, C.-H. Yang, M.-L. Kuo, J.-H. Lin, C.-K. Tseng, and C.-Y. Chang, *J. Electrochem. Soc.*, **154**, G155 (2007).
11. S. J. Whang, S. J. Lee, F. Gao, N. Wu, C. X. Zhu, J. S. Pan, L. J. Tang, and D. L. Kwong, in *International Electron Devices Meeting Technical Digest*, p. 307 (2004).
12. M. M. Frank, S. J. Koester, M. Copel, J. A. Ott, V. K. Paruchuri, H. Shang, and R. Loesing, *Appl. Phys. Lett.*, **89**, 112905 (2006).
13. N. Wu, Q. Zhang, D. S. H. Chan, N. Balasubramanian, and C. Zhu, *IEEE Electron Device Lett.*, **25**, 631 (2004).
14. E. H. Nicollian and J. R. Brews, *MOS (Metal Oxide Semiconductor) Physics and Technology*, John Wiley & Sons, Inc., New York (1982).
15. C. U. S. Larsson and A. S. Flodstrom, *Phys. Rev. B*, **43**, 9281 (1991).
16. C. Ehlers, U. Konig, G. Staikov, and J. W. Schultze, *Electrochim. Acta*, **47**, 379 (2001).
17. S. Rivillon, Y. J. Chabal, F. Amy, and A. Kahn, *Appl. Phys. Lett.*, **87**, 253101 (2005).
18. C.-C. Cheng, C.-H. Chien, G.-L. Luo, J.-C. Liu, C.-Y. Chang, C.-C. Kei, D.-R. Liu, and C.-N. Hsiao, *Chem. Vap. Deposition*, Submitted.
19. D. R. Lide, *CRC Handbook of Chemistry and Physics: A Ready-Reference Book of Chemical and Physical Data*, 84th ed., CRC Press, Boca Raton, FL (2003).
20. D. E. Grey, *American Institute of Physics Handbook*, American Institute of Physics, New York (1982).
21. Y.-S. Min, Y. J. Cho, and C. S. Hwang, *Chem. Mater.*, **17**, 626 (2005).
22. J. W. Seo, Ch. Dieker, J.-P. Locquet, G. Mavrou, and A. Dimoulas, *Appl. Phys. Lett.*, **87**, 221906 (2005).
23. K. Prabhakaran, F. Maeda, Y. Watanabe, and T. Ogino, *Appl. Phys. Lett.*, **76**, 2244 (2000).
24. K. Prabhakaran and T. Ogino, *Surf. Sci.*, **387**, L1068 (1997).
25. C.-C. Cheng, C.-H. Chien, C.-W. Chen, S.-L. Hsu, C.-H. Yang, and C.-Y. Chang, *J. Electrochem. Soc.*, **153**, F160 (2006).
26. A. Dimoulas, G. Vellianities, G. Mavrou, E. K. Evangelou, and A. Sotiropoulos, *Appl. Phys. Lett.*, **86**, 223507 (2005).
27. J. Vanhellemont and E. Simoen, *J. Electrochem. Soc.*, **154**, H572 (2007).
28. P. Batude, X. Garros, L. Clavelier, C. Le Royer, J. M. Hartmann, V. Loup, P. Besson, L. Vandroux, Y. Campidelli, S. Deleonibus, et al., *J. Appl. Phys.*, **102**, 034514 (2007).
29. J. J.-H. Chen, N. A. Bojarczuk, Jr., H. Shang, M. Copel, J. B. Hannon, J. Karasinski, E. Preisler, S. K. Banerjee, and S. Guha, *IEEE Trans. Electron Devices*, **51**, 1441 (2004).
30. E. K. Evangelou, G. Mavrou, A. Dimoulas, and N. Konofaos, *Solid-State Electron.*, **51**, 164 (2007).
31. T. Maeda, M. Nishizawa, Y. Morita, and S. Takagi, *Appl. Phys. Lett.*, **90**, 072911 (2007).
32. V. V. Afanas'ev, Y. G. Fedorenko, and A. Stesmans, *Appl. Phys. Lett.*, **87**, 032107 (2005).

Downloaded on 2014-04-25 to IP 140.113.38.11 address. Redistribution subject to ECS terms of use (see ecsdl.org/site/terms_use) unless CC License in place (see abstract).